Journal of Sound and Vibration (1998) **212**(5), 807–828

VIBRATION ANALYSIS OF ROTATING CANTILEVER BEAMS

H. H. Yoo and S. H. Shin

Department of Mechanical Engineering, Hanyang University, Haengdang-Dong 17, *Sungdong-Gu, Seoul* 133-791, *Korea*

(*Received* 9 *September* 1996, *and in final form* 12 *December* 1997)

Equations of motion of a rotating cantilever beam are derived based on a new dynamic modelling method in this paper. The derived equations (governing stretching and bending motions), which are coupled through gyroscopic coupling terms, are all linear, so they can be directly used for the vibration analysis including the coupling effect, which could not be considered in the conventional modelling method. With the coupling effect ignored, the analysis results are consistent with the results obtained by the conventional modelling method. With the coupling effect considered, eigenvalue loci veerings and mode shape variations could be observed through numerical study. Generally, when the rotating speed increases up to a certain value, the analysis results including the coupling effect show significant difference compared to the results ignoring the coupling effect. A modal formulation method is also introduced in this study to calculate the tuned angular speed of a rotating beam at which resonance occurs.

1. INTRODUCTION

Vibration analysis of a rotating cantilever beam is an important and peculiar subject of study in mechanical engineering. There are many engineering examples which can be idealized as rotating cantilever beams, such as turbine blades, turbo-engine blades, and helicopter blades. For the proper design of the structures, their vibration characteristics, which are natural frequencies and mode shapes, should be well identified. Compared to the vibration characteristics of non-rotating structures, those of rotating structures often vary significantly. The variation results from the stretching induced by the centrifugal inertia force due to the rotational motion. The stretching causes the increment of the bending stiffness of the strucutre, which naturally results in the variation of natural frequencies and mode shapes.

Study of the natural frequency variation of rotating beams originated from the work by Southwell and Gough [1]. Based on the Rayleigh energy theorem, they suggested a simple equation (well-known as the Southwell equation) to estimate the natural frequencies of rotating cantilever beams. The study was later extended by Liebers [2] and Theodorsen [3]. Mode shape variations, however, could not be obtained with the method. Moreover, as the rotating angular speed increases, the accuracy of the method deteriorates. To obtain more accurate natural frequencies, Schilhansl [4] derived a linear partial differential equation which governs only bending motions of a rotating beam. By using the equation along with the Ritz method, more accurate coefficients for the Southwell equation were obtained analytically. However, mode shapes were not obtained since the amount of calculation was large at the time. As computer and numerical methods progressed, such calculation could be performed, and mode shapes as well as more accurate natural

0022–460X/98/200807 + 22 $25.00/0/sv971469

frequencies were obtained by several researchers [5–10]. Recent research has covered more complex effects [11–13]. A large amount of literature relating to this subject can be found (see, for instance, [14, 15]).

The most popular modelling method that is being used for the *transient* analysis of structure is the classical linear modelling method [16, 17]. This modelling method has several merits such as ease of formulation, saving computational effort, and coordinate reduction (which is probably the most critical factor for transient analysis). This modelling method, however, would provide incorrect modal characteristics for the rotating structure since it is based on the assumption of geometric linearity. Geometric nonlinear terms, which are truncated from the linear modelling method, play important roles in correctly estimating the modal characteristics. Therefore, for the vibration analysis of a rotating beam, a different dynamic modelling method needs to be employed.

The conventional modelling method employed for the vibration analysis of a rotating beam can be summarized as follows. First, full sets of nonlinear differential equations of motion are derived. From the equation governing stretching motion, an equation relating the axial strain to the centrifugal inertia forces is obtained by truncating the rest of the terms. Then the centrifugal inertia forces is substituted for the axial strain in the equations governing bending motions. Now, by truncating all nonlinear terms from the resulting bending equations, linear equations for the bending vibration analysis are obtained. Since the equation governing stretching motion is not used any longer for the vibration analysis, the coupling effect between stretching and bending motions is always ignored. Therefore, this conventional modelling method is valid only if the coupling effect is actually negligible.

Recently, a new dynamic modelling method which employs a hybrid set of deformation variables was introduced in [18, 19]. Full sets of linear equations of motion were derived in the new dynamic modelling method. The linear equations, different from those of the classical linear modelling method, were shown to provide proper stiffness vartiation due to rotational motion. Since all the equations of the modelling method are linear, they could be directly used (without the substitution procedure) for the vibration analysis. This modelling method is simpler, more consistent, and more rigorous than the conventional modelling method. Moreover, the coupling effect between stretching and bending motions can be considered for the vibration analysis. Therefore, the importance of the coupling effect, if it exists, can be investigated with the equations obtained from the modelling method. Based on the modelling method [18, 19], transient analyses were performed and the integrity of the modelling method was proved. The purpose of this paper is to perform the modal analysis of rotating cantilever beams based on the modelling method.

2. EQUATIONS OF MOTION

In this section, equations of motion of a rotating cantilever beam are derived based on the following assumptions. The beam has homogeneous and isotropic material properties. The elastic and centroidal axes in the cross section of a beam coincide so that effects due to eccentricity are not considered. The beam has a slender shape so that shear and rotary inertia effects are neglected. The beam is attached to a hub which rotates with a constant angular velocity. These assumptions result in simplified equations of motion with which the main issues of this study (the stiffening effect and modal characteristics variation due to rotation) are effectively investigated. However, more complex effects, if necessary, can be included in the modelling method.

Figure 1 shows the configuration of a rotating beam attached to a hub. The elastic deformation of the beam is denoted as $\vec{u}$ in the figure. The vector has three components in 3-D space which are expressed by three scalar variables. Conventionally, three Cartesian

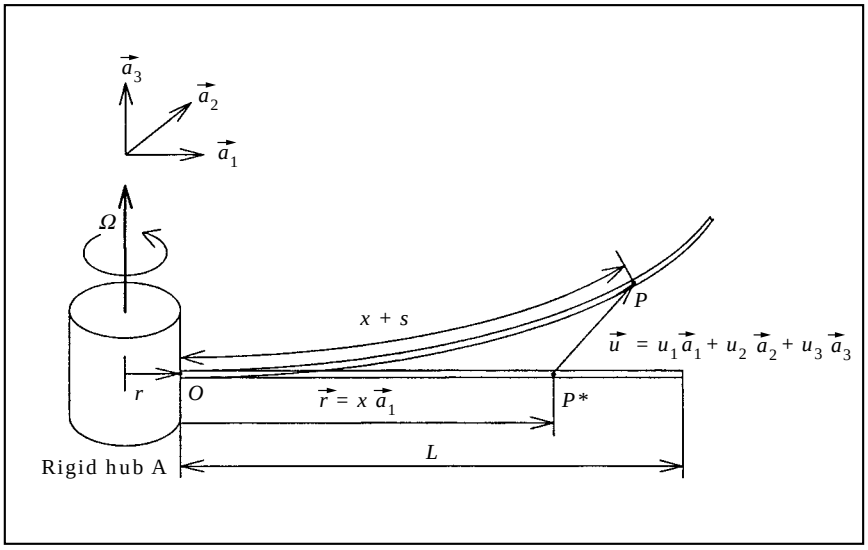

Figure 1. Configuration of a rotating cantilever beam.

deformation variables are used. In the present study, however, a non-Cartesian variable s denoting the arc-length stretch is used instead of u_1 which denotes the Cartesian distance measure of a generic point in the axial direction of the undeformed configuration of the beam. Thus, a hybrid set (Cartesian variables u_2 and u_3 along with the non-Cartesian variable) is employed to derive the equations of motion. In the present work, the Rayleigh–Ritz assumed mode method is used to approximate the hybrid set of variables.

$$s(x, t) = \sum_{j=1}^{\mu} \phi_{1j}(x) q_j(t) \tag{1}$$

$$u_2(x, t) = \sum_{j=1}^{\mu} \phi_{2j}(x) q_j(t) \tag{2}$$

$$u_3(x, t) = \sum_{j=1}^{\mu} \phi_{3j}(x) q_j(t) \tag{3}$$

where ϕ_{1j}, ϕ_{2j}, and ϕ_{3j} are spatial functions. Any compact set of functions which satisfy the boundary conditions of the cantilever beam, can be used. q_js are generalized coordinates and μ is the total number of modal coordinates. For the convenience of formalism, s, u_2, and u_3 explicitly use the same number of coordinates, μ. However, they do not use the same coordinates. For instance, ϕ_{1j} is not zero only if $j \leqslant \mu_1$; ϕ_{2j} is not zero only if $\mu_1 < j \leqslant \mu_1 + \mu_2$ and ϕ_{3j} is not zero only if $\mu_1 + \mu_2 < j \leqslant \mu_1 + \mu_2 + \mu_3$. In other words, μ_1, μ_2, and μ_3 denote the actual numbers of generalized coordinates for s, u_2, and u_3, respectively. μ is the total sum of μ_1, μ_2, and μ_3.

Based on the assumptions given in the beginning of this section, the strain energy can be written as

$$U = \frac{1}{2}\int_0^L EA\left(\frac{\partial s}{\partial x}\right)^2 \mathrm{d}x + \frac{1}{2}\int_0^L EI_{zz}\left(\frac{\partial^2 u_2}{\partial x^2}\right)^2 \mathrm{d}x + \frac{1}{2}\int_0^L EI_{yy}\left(\frac{\partial^2 u_3}{\partial x^2}\right)^2 \mathrm{d}x \tag{4}$$

where E denotes Young's modulus, A is the cross-sectional area, I_{zz} and I_{yy} are the second area moments of the cross section, and L is the undeformed length of the beam. The first term in equation (4) represents the exact stretching energy of the beam since s represents the exact stretch of the beam. With the quadratic form of strain energy given in equation (4), the generalized active forces can be obtained by the following equation.

$$F_i = -\frac{\partial U}{\partial q_i} \qquad (i = 1, 2, \ldots, \mu). \tag{5}$$

The use of s results in linear generalized active forces. It, however, complicates the formulation of generalized inertia forces in the equations of motion.

The velocity of a generic point P can be obtained as follows.

$$\vec{v}^P = \vec{v}^O + \vec{\omega}^A \times (\vec{r} + \vec{u}) + {}^A\vec{v}^P \tag{6}$$

where O is a reference point identifying a point fixed in the rigid frame A; $\vec{v}^O$ is the velocity of point O; $\vec{\omega}^A$ is the angular velocity of the frame A; $\vec{r}$ is a position vector from O to the location of P in the undeformed body; $\vec{u}$ is the elastic deformation vector ; and ${}^A\vec{v}^P$ is the relative velocity of P with respect to frame A obtained by taking the time derivative of $\vec{u}$ in frame A. When the rigid hub (of radius r) rotates at a constant angular speed Ω, these vectors can be expressed as follows.

$$\vec{r} = x\vec{a}_1 \tag{7}$$

$$\vec{u} = u_1\vec{a}_1 + u_2\vec{a}_2 + u_3\vec{a}_3 \tag{8}$$

$$\vec{v}^O = r\Omega\vec{a}_2 \tag{9}$$

$$\vec{\omega}^A = \Omega\vec{a}_3 \tag{10}$$

where $\vec{a}_1$, $\vec{a}_2$, and $\vec{a}_3$ are orthogonal unit vectors fixed in A. By substituting equations (7)–(10) into equation (6), the velocity of point P can be expressed as

$$\vec{v}^P = (\dot{u}_1 - \Omega u_2)\vec{a}_1 + [\dot{u}_2 + \Omega(r + x + u_1)]\vec{a}_2 + \dot{u}_3\vec{a}_3 \tag{11}$$

u_1 and $\dot{u}_1$, appearing in equation (11), need to be expressed in terms of s, u_2, u_3, and their time derivatives (since s instead of u_1 approximated). The geometric relation between the arc-length stretch s and the Cartesian variables is given as follows [20]:

$$x + s = \int_0^x \left[\left(1 + \frac{\partial u_1}{\partial \sigma}\right)^2 + \left(\frac{\partial u_2}{\partial \sigma}\right)^2 + \left(\frac{\partial u_3}{\partial \sigma}\right)^2\right]^{1/2} \mathrm{d}\sigma. \tag{12}$$

Using a binomial expansion of the integrand of equation (12), it can be shown to give

$$s = u_1 + \frac{1}{2}\int_0^x \left[\left(\frac{\partial u_2}{\partial \sigma}\right)^2 + \left(\frac{\partial u_3}{\partial \sigma}\right)^2\right] \mathrm{d}\sigma + (\text{Higher Degree Terms}). \tag{13}$$

Equation (13) is convenient for the derivation of the linear equations of motion. Differentiation of the above equation with respect to time is given as

$$\dot{s} = \dot{u}_1 + \int_0^x \left[\left(\frac{\partial \dot{u}_2}{\partial \sigma} \right) \left(\frac{\partial u_2}{\partial \sigma} \right) + \left(\frac{\partial \dot{u}_3}{\partial \sigma} \right) \left(\frac{\partial u_3}{\partial \sigma} \right) \right] \mathrm{d}\sigma + (\text{Higher Degree Terms}). \tag{14}$$

Using equations (11) and (14), the partial derivative of the velocity of P with respect to the generalized speed $\dot{q}_i$ (often called as the partial velocity) can be obtained as

$$\frac{\partial \vec{v}^P}{\partial \dot{q}_i} = \left[\phi_{1i} - \sum_{j=1}^{\mu} \left(\int_0^x \phi_{2i,\eta}\, \phi_{2j,\eta}\, \mathrm{d}\eta \right) q_j - \sum_{j=1}^{\mu} \left(\int_0^x \phi_{3i,\eta}\, \phi_{3j,\eta}\, \mathrm{d}\eta \right) q_j \right] \vec{a}_1 + \phi_{2i}\, \vec{a}_2 + \phi_{3i}\, \vec{a}_3 \tag{15}$$

where η after comma denotes partial differentiation with respect to the dummy variable η. By differentiating equation (11) with respect to time, the acceleration of P can be obtained as follows.

$$\vec{a}^P = [\ddot{u}_1 - 2\Omega \dot{u}_2 - \Omega^2 (r + x + u_1)] \vec{a}_1 + (\ddot{u}_2 + 2\Omega \dot{u}_1 - \Omega^2 u_2) \vec{a}_2 + \ddot{u}_3\, \vec{a}_3. \tag{16}$$

Based on the assumption of neglecting rotary inertia effect, the generalized inertia forces for a beam can be derived by using the following equation.

$$F_i^* = -\int_0^L \rho \left(\frac{\partial \vec{v}^P}{\partial \dot{q}_i} \right) \cdot \vec{a}^P \, \mathrm{d}x \qquad (i = 1, 2, \ldots, \mu) \tag{17}$$

where ρ represents the mass per unit length of the beam. By linearizing the generalized inertia forces, equations of motion are finally obtained as follows.

$$\sum_{j=1}^{\mu} \left[\left(\int_0^L \rho \phi_{1i}\, \phi_{1j}\, \mathrm{d}x \right) \ddot{q}_j - 2\Omega \left(\int_0^L \rho \phi_{1i}\, \phi_{2j}\, \mathrm{d}x \right) \dot{q}_j - \Omega^2 \left(\int_0^L \rho \phi_{1i}\, \phi_{1j}\, \mathrm{d}x \right) q_j \right.$$

$$\left. + \left(\int_0^L EA \phi_{1i,x}\, \phi_{1j,x}\, \mathrm{d}x \right) q_j \right] = \Omega^2 \int_0^L \rho x \phi_{1i}\, \mathrm{d}x + r\Omega^2 \int_0^L \rho \phi_{1i}\, \mathrm{d}x \tag{18}$$

$$\sum_{j=1}^{\mu} \left[\left(\int_0^L \rho \phi_{2i}\, \phi_{2j}\, \mathrm{d}x \right) \ddot{q}_j - \Omega^2 \left(\int_0^L \rho \phi_{2i}\, \phi_{2j}\, \mathrm{d}x \right) q_j + \left(\int_0^L EI_{zz}\, \phi_{2i,xx}\, \phi_{2j,xx}\, \mathrm{d}x \right) q_j \right.$$

$$+ \Omega^2 \left\{ r \left(\int_0^L \rho (L - x) \phi_{2i,x}\, \phi_{2j,x}\, \mathrm{d}x \right) q_j + \left(\int_0^L \frac{\rho}{2} (L^2 - x^2) \phi_{2i,x}\, \phi_{2j,x}\, \mathrm{d}x \right) q_j \right\}$$

$$\left. + 2\Omega \left(\int_0^L \rho \phi_{2i}\, \phi_{1j}\, \mathrm{d}x \right) \dot{q}_j \right] = 0 \tag{19}$$

$$\sum_{j=1}^{\mu}\left[\left(\int_0^L \rho\phi_{3i}\,\phi_{3j}\,\mathrm{d}x\right)\ddot{q}_j + \left(\int_0^L EI_{yy}\,\phi_{3i,xx}\,\phi_{3j,xx}\,\mathrm{d}x\right)q_j + \Omega^2\left\{r\left(\int_0^L \rho(L-x)\phi_{3i,x}\,\phi_{3j,x}\,\mathrm{d}x\right)q_j + \left(\int_0^L \frac{\rho}{2}(L^2-x^2)\phi_{3i,x}\,\phi_{3j,x}\,\mathrm{d}x\right)q_j\right\}\right] = 0. \tag{20}$$

Since the total number of generalized coordinates is μ, equations (18)–(20) consist of μ equations.

3. MODAL ANALYSIS

3.1. FLAPWISE BENDING VIBRATION ANALYSIS

The flapwise bending vibration of the rotating beam is governed by equation (20) which is not coupled with equations (18) and (19). Several variables (e.g. ρ, L, I_{yy}, Ω, t, and x) are involved in equation (20) in which cross sectional properties of a beam (such as area and area moment of inertia) may vary arbitrarily along the longitudinal axis. If the cross sectional properties remain constant, it is useful to rewrite the equation in a dimensionless form. To achieve this, the following dimensionless variables are introduced.

$$\tau \triangleq \frac{t}{T} \tag{21}$$

$$\xi \triangleq \frac{x}{L} \tag{22}$$

$$\theta_j \triangleq \frac{q_j}{L} \tag{23}$$

$$\delta \triangleq \frac{r}{L} \tag{24}$$

$$\gamma \triangleq T\Omega \tag{25}$$

TABLE 1

Convergence of natural frequencies vs number of modes

No. of modes	First	Second	Third
1	108·37	—	—
2	105·73	254·18	—
3	103·65	253·52	407·20
4	102·57	251·84	407·13
5	101·98	249·93	407·13
6	101·62	249·47	401·35
7	101·40	248·83	401·31
8	101·26	248·59	400·42
9	101·20	248·44	400·19
10	101·17	248·38	400·15

$\delta = 0$, $\gamma = 100$.

where

$$T \triangleq \left(\frac{\rho L^4}{EI_{yy}}\right)^{1/2}.$$

Introducing these dimensionless variables into equation (20), one obtains:

$$\sum_{j=1}^{\mu} [M_{ij}^{33}\,\ddot{\theta}_j + K_{ij}^{B3}\,\theta_j + \gamma^2 K_{ij}^{G3}\,\theta_j] = 0 \tag{26}$$

where two dots over the symbol θ_j means double differentiation of θ_j with respect to τ (dimensionless time) and

$$M_{ij}^{ab} \triangleq \int_0^1 \psi_{ai}\,\psi_{bj}\,\mathrm{d}\xi \tag{27}$$

$$K_{ij}^{Ba} \triangleq \int_0^1 \psi_{ai,\xi\xi}\,\psi_{aj,\xi\xi}\,\mathrm{d}\xi \tag{28}$$

$$K_{ij}^{Ga} \triangleq \int_0^1 (1-\xi)\psi_{ai,\xi}\,\psi_{aj,\xi}\,\mathrm{d}\xi + \frac{1}{2}\int_0^1 (1-\xi^2)\psi_{ai,\xi}\,\psi_{aj,\xi}\,\mathrm{d}\xi \tag{29}$$

where ψ_{aj} is a function of ξ, and has the same functional value as ϕ_{ai}.

From equation (26), an eigenvalue problem for the flapwise bending vibration of a rotating cantilever beam can be formulated by assuming that the θ_js are harmonic

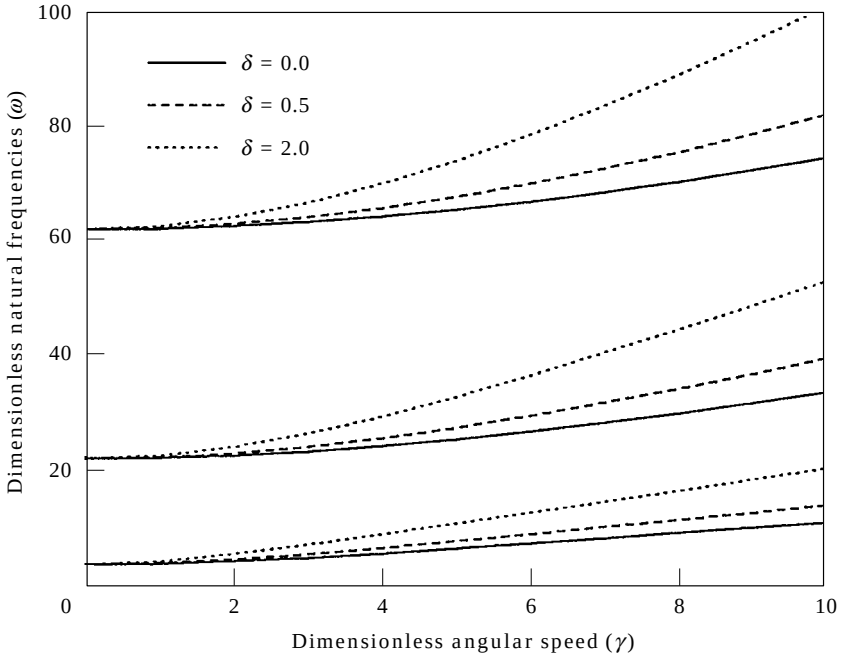

Figure 2. Flapwise bending natural frequency variations.

TABLE 2

Comparison of first and second natural frequencies in the flapwise bending vibration

	First natural frequency		Second natural frequency	
γ	Present	Ref. [9]	Present	Ref. [9]
0	3·5160	3·5160	22·035	22·035
1	3·6816	3·6817	22·181	22·181
2	4·1373	4·1373	22·615	22·615
3	4·7973	4·7973	23·320	23·320
4	5·5850	5·5850	24·273	24·273
5	6·4495	6·4495	25·446	25·446
6	7·3604	7·3604	26·809	26·809
7	8·2996	8·2996	28·334	28·334
8	9·2568	9·2568	29·995	29·995
9	10·226	10·226	31·771	31·771
10	11·202	11·202	33·640	33·640

$\delta = 0$.

functions of τ. If θ represents a column matrix which has θ_j s as its elements, it can be expressed as

$$\theta = e^{j\omega\tau}\Theta \tag{30}$$

where j represents a imaginary number, ω is the ratio of the flapwise bending natural frequency to the reference frequency (inverse of T), and Θ is a constant

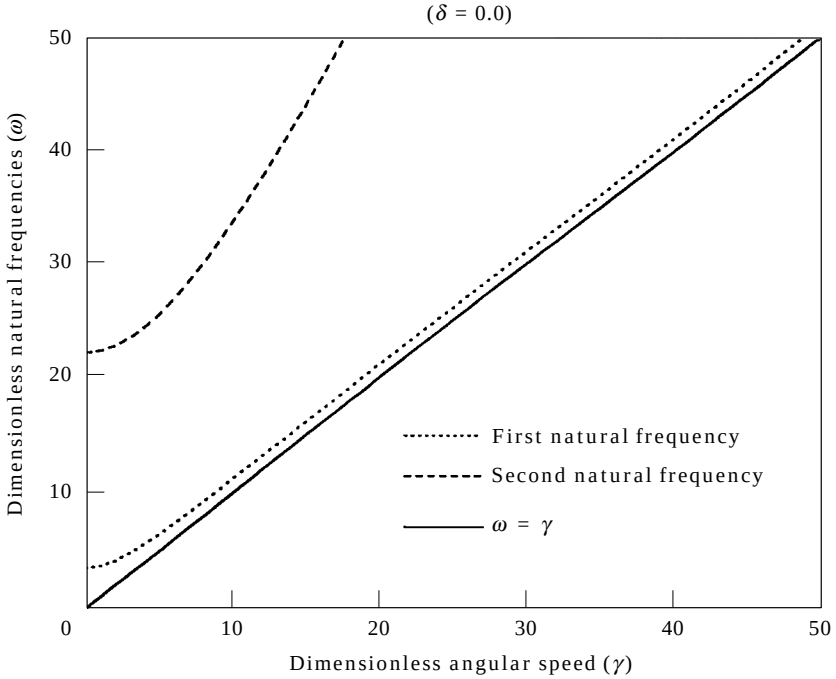

Figure 3. Angular speed and flapwise bending natural frequencies.

column matrix characterizing the deflection shape for synchronous motion. This yields

$$\omega^2 \mathbf{M}\Theta = \mathbf{K}^F\Theta \tag{31}$$

where $\mathbf{M}$ and $\mathbf{K}^F$ are square matrices, whose respective elements M_{ij} and K_{ij}^F are defined as

$$M_{ij} \triangleq M_{ij}^{33} \tag{32}$$

$$K_{ij}^F \triangleq K_{ij}^{B3} + \gamma^2 K_{ij}^{G3}. \tag{33}$$

In order to obtain accurate numerical results, several assumed modes are used to construct the matrices defined in equations (32) and (33). Table 1 shows a typical trend of converging natural frequencies for a rotating beam with zero hub radius. The natural frequencies converge rapidly as more modes are added. In this study, ten assumed modes

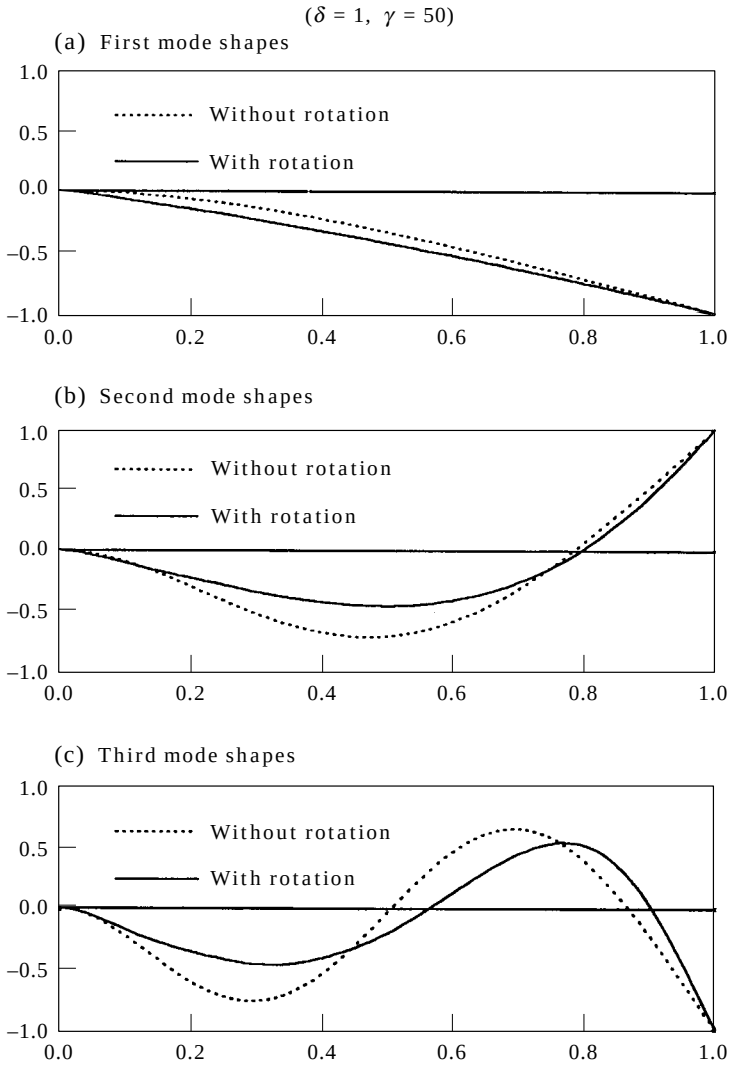

Figure 4. Flapwise bending mode shape variations due to rotation.

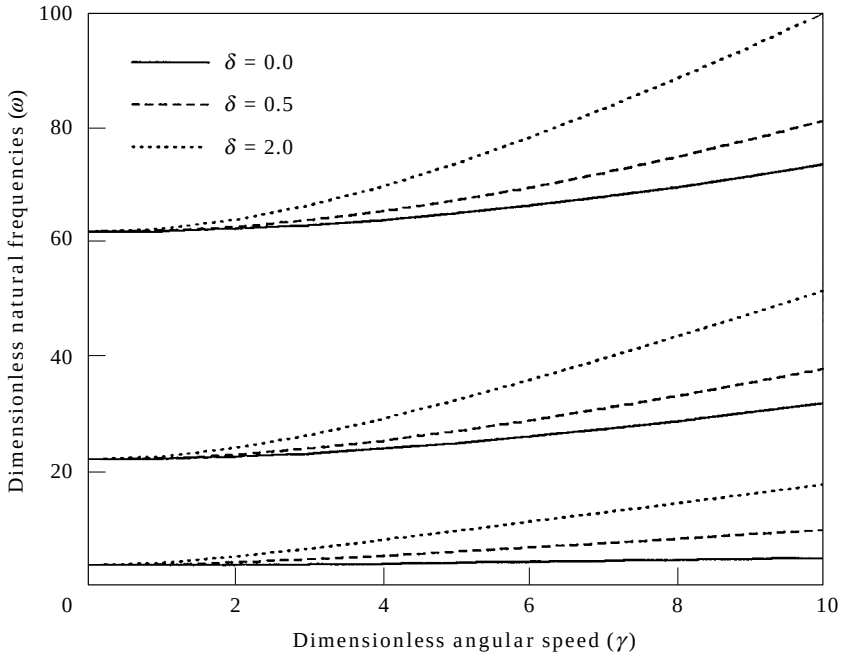

Figure 5. Chordwise bending natural frequency variations.

are used to obtain three lowest natural frequencies and mode shapes. The lowest ten polynomial comparison functions are used for the assumed modes.

The flapwise bending natural frequency variations are shown in Figure 2. The lowest three natural frequencies are plotted for three cases of hub radius ratio δ. The dimensionless natural frequencies (ω) increase as the angular speed ratio (γ) increases, and the increasing rates (the slope of the trajectory) become larger as the hub radius ratio (δ) becomes larger. This results from the centrifugal inertia force which increases as the angular speed and the hub radius increase.

In Table 2, numerical results obtained by using the present modelling method are compared to those in [9] which provides some analytical solutions for the flapwise bending

TABLE 3

Comparison of the natural frequencies in the chordwise bending vibration

		First natural frequency		Second natural frequency	
δ	γ	Present	Ref. [5]	Present	Ref. [5]
0	2	3·62	3·61	22·5	22·5
	10	5·05	5·05	32·1	32·1
	50	10·5	10·5	116	116
1	2	4·40	4·40	23·3	23·3
	10	13·3	13·3	43·2	43·2
	50	61·6	61·6	182	182
5	2	6·65	6·65	26·1	26·1
	10	27·7	27·7	71·4	71·4
	50	136	136	332	332

vibration. The results of the present modelling method shows a $< 0.02\%$ difference from the analytical solutions, which implies no practical difference.

Resonance will occur if the rotating frequency of the beam matches its own natural frequency. The anular speed causing the resonance is often called the tuned angular speed. In Figure 3, the trajectories of the lowest two natural frequencies (for $\delta = 0$) and the straight line of $\omega = \gamma$ are plotted, and no tuned speed can be found. The increment of δ will cause the increment of the slope of the natural frequency trajectories. Thus, one can conclude that no tuned angular speed exists at any hub radius ratio in the flapwise bending vibration of the rotating cantilever beam.

The mode shape variations of the rotating beam are shown in Figure 4. The dotted lines represent the mode shapes of the beam with no rotational motion, and the solid lines represent those of the beam with rotational motion ($\gamma = 50$, about 12 times of the first bending natural frequency). Noticeable difference exists between the two sets of lines. Information about mode shape variation (e.g., position of nodal points) may be utilized usefully for the control of a rotating beam.

3.2. CHORDWISE BENDING VIBRATION ANALYSIS IGNORING THE COUPLING EFFECT

Equation (19) is coupled with equation (18) through gyroscopic coupling terms. The coupling terms are often assumed negligible and ignored in this section. This assumption is usually reasonable since the first stretching natural frequency of an Eulerian beam is far separated from the first bending natural frequency. With this assumption, equation (19) can be simplified as

$$\sum_{j=1}^{\mu}\left[\left(\int_0^L \rho\phi_{2i}\,\phi_{2j}\,\mathrm{d}x\right)\ddot{q}_j - \Omega^2\left(\int_0^L \rho\phi_{2i}\,\phi_{2j}\,\mathrm{d}x\right)q_j + \left(\int_0^L EI_{zz}\,\phi_{2i,xx}\,\phi_{2j,xx}\,\mathrm{d}x\right)q_j\right]$$

$$+\,\Omega^2\left\{r\left(\int_0^L \rho(L-x)\phi_{2i,x}\,\phi_{2j,x}\,\mathrm{d}x\right)q_j + \left(\int_0^L \frac{\rho}{2}(L^2-x^2)\phi_{2i,x}\,\phi_{2j,x}\,\mathrm{d}x\right)q_j\right\} = 0 \qquad (34)$$

To write equation (34) in a dimensionless form, the dimensionless variables defined in equations (21)–(25) are again used. However, instead of I_{yy}, I_{zz} should be used to define T in equation (25). Introducing the dimensionless variables into equation (34), one obtains

$$\sum_{j=1}^{\mu}\left[M_{ij}^{22}\,\ddot{\theta}_j + K_{ij}^{B2}\,\theta_j + \gamma^2(-M_{ij}^{22} + K_{ij}^{G2})\theta_j\right] = 0. \qquad (35)$$

From equation (35), an eigenvalue problem for the chordwise bending vibration of a rotating cantilever beam can be formulated as

$$\omega^2\mathbf{M}\Theta = \mathbf{K}^C\Theta \qquad (36)$$

where M_{ij} and K_{ij}^C are defined as

$$M_{ij} \triangleq M_{ij}^{22} \qquad (37)$$

$$K_{ij}^C \triangleq K_{ij}^{B2} + \gamma^2(K_{ij}^{G2} - M_{ij}^{22}). \qquad (38)$$

If I_{yy} is equal to I_{zz}, the elements of the stiffness matrix defined in equation (38) is less than the ones of the stiffness matrix defined in equation (33) by $\gamma^2 M_{ij}^{22}$. Thus the dimensionless chordwise bending natural frequencies are less than the dimensionless flapwise bending natural frequencies if the structural rigidities in two bending directions are the same. Actually, the relation between the chordwise bending natural frequencies and flapwise

bending natural frequencies can be easily derived from the relation of stiffness matrices. If $\mathbf{V}$ is the normalized modal matrix obtained from the flapwsie bending modal equation,

$$\mathbf{V}^T\mathbf{M}\mathbf{V} = \mathbf{I} \tag{39}$$

$$\mathbf{V}^T\mathbf{K}^F\mathbf{V} = \mathbf{D}^F \tag{40}$$

where $\mathbf{I}$ denotes an identity matrix, and $\mathbf{D}^F$ is a diagonal matrix whose elements are the squares of the flapwise bending natural frequencies. If the chordwise bending stiffness matrix is now pre and post multiplied by the same normalized matrix, the following relation holds.

$$\mathbf{V}^T\mathbf{K}^C\mathbf{V} = \mathbf{D}^C = \mathbf{D}^F - \gamma^2\mathbf{I} \tag{41}$$

where $\mathbf{D}^C$ is an diagonal matrix whose elements are the squares of the chordwise bending natural frequencies. Thus the squares of the dimensionless chordwise bending natural frequencies are less than the squares of the dimensionless flapwise bending natural frequencies by the squares of the dimensionless angular speed.

$$\omega_{ci}^2 = \omega_{fi}^2 - \gamma^2 \tag{42}$$

where ω_{ci} and ω_{fi} denote the ith dimensionless chordwise and flapwise bending natural frequencies respectively. This relation was originally introduced in [12].

The dimensionless chordwise bending natural frequency variations are shown in Figure 5. The lowest three natural frequencies are plotted for three cases of hub radius ratios. To obtain the result, 10 assumed modes are used. As can be expected intuitively, the natural frequencies increase as the angular speed increases, and the increasing rate becomes larger as the hub radius ratio becomes larger. In Table 3, the first and second natural frequencies obtained through the present analysis are compared to those of [5], for which the typical modelling procedure along with a finite element method is employed. Most of the two sets of results show only trivial discrepancy. This shows that the present modelling method is qualitatively equivalent to the conventional modelling method if the coupling effect is ignored from the present modelling method. In Table 4, the chordwise bending natural frequencies are compared to the flapwise bending natural frequencies. The table shows that the dimensionless chordwise natural frequencies obtained by using equation (42) match well with the ones which are obtained directly from the modal analysis.

TABLE 4

Comparison of the first chordwise natural frequencies and the first flapwise natural frequencies

δ	γ	Flapwise	Chordwise [by equation (36)]	Chordwise [by equation (42)]
0	2	4·14	3·62	3·62
	10	11·2	5·05	5·04
	50	51·1	10·5	10·5
1	2	4·83	4·40	4·40
	10	16·6	13·3	13·2
	50	79·4	61·6	61·7
5	2	6·94	6·65	6·65
	10	29·5	27·7	27·8
	50	145	136	136

In Figure 6, three trajectories of the first natural frequency (for $\delta = 0$, $\delta = 1$, and $\delta = 5$) are plotted. The tuned angular speed occurs at $\gamma = 3{\cdot}88$ for $\delta = 0$, but it does not exist for $\delta = 1$ or $\delta = 5$. Therefore, there exists a limit value of hub radius ratio only under which the tuned angular speed exists. The ratio is called, herein, the critical hub radius ratio. A natural frequency trajectory should cross the straight line of $\omega = \gamma$ to have a tuned angular speed. This crossing occurs when the asymptotic slope of the dimensionless natural frequency trajectory is <1. As γ becomes larger, the first term of equation (38) becomes negligible compared to other terms. By ignoring the first term, the eigenvalue problem given in equation (36) can be re-formulated as follows.

$$\lambda^2 \mathbf{M\Theta} = \mathbf{K^*\Theta} \tag{43}$$

where

$$\lambda \triangleq \frac{\omega}{\gamma} \tag{44}$$

$$K_{ij}^* \triangleq K_{ij}^{G2} - M_{ij}^{22}. \tag{45}$$

As defined in equation (44), λ represents the slope of a dimensionless natural frequency trajectory. Therefore, if $\lambda < 1$, the tuned angular speed exists. Trajectories of λs with varying hub radius ratios are shown in Figure 7. $\lambda < 1$ only occurs with the first natural frequency. The approximate value of the critical hub radius, at which $\lambda = 1$ is $0{\cdot}655$.

λ defined in equation (44) is related to the coefficient of the Southwell equation, which is often written as

$$\Omega_{ni}^2 = \Omega_{bi}^2 + S_i \Omega^2 \tag{46}$$

where Ω_{ni} and Ω_{bi} respectively denote the ith natural frequency of a beam with and without rotational motion, Ω is the angular speed of the beam, and S_i is the Southwell coefficient.

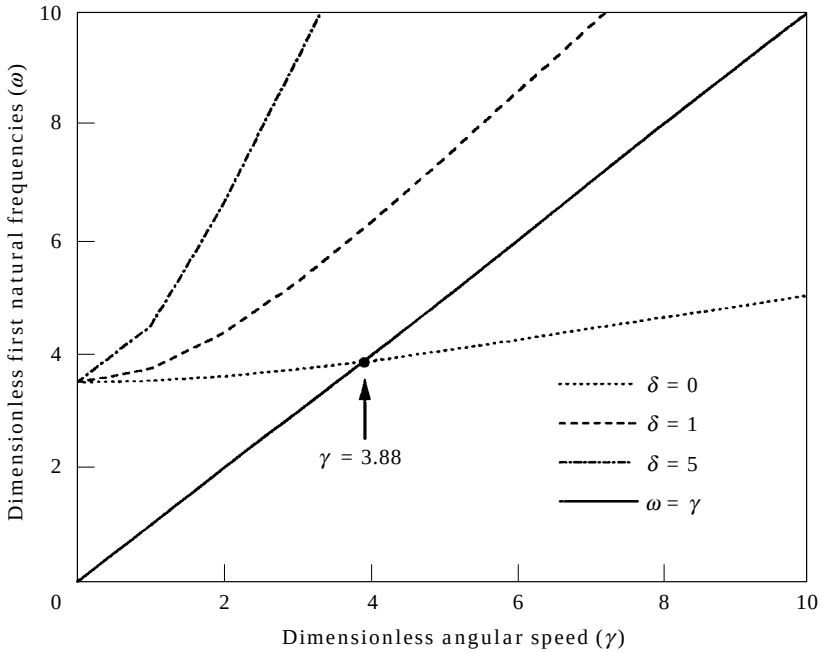

Figure 6. Tuned angular speed in chordwise bending vibration.

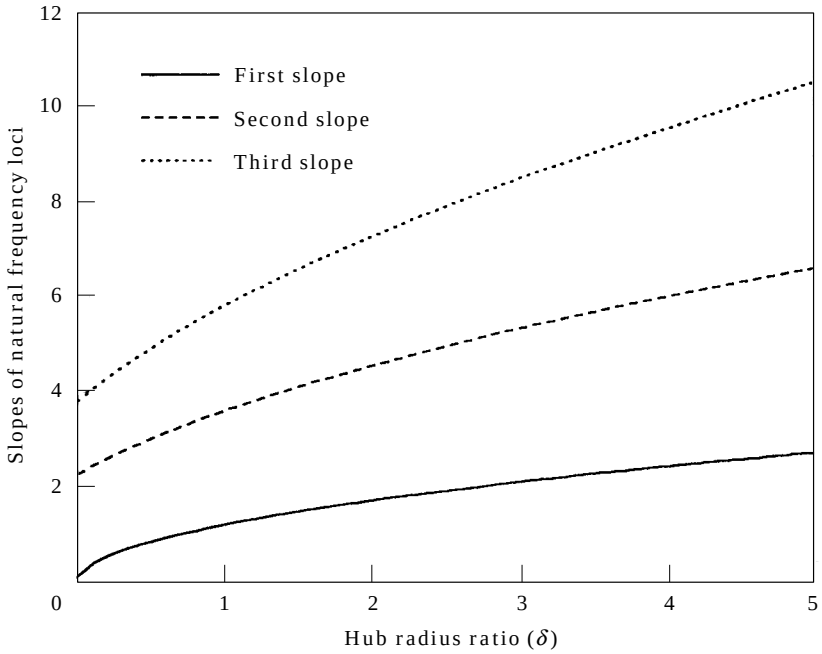

Figure 7. Slopes of chordwise bending natural frequency loci.

From the equation, it is easily inferred that the slope (λ) of the dimensionless natural frequency is equal to $S_i^{1/2}$. Therefore, by solving the eigenvalue problem of equation (43), the Southwell coefficients with varying δ can be calculated. The trajectories of Southwell coefficients vs hub radius ratio δ are shown in Figure 8. Since the trajectories are almost straight, they are conventionally represented by linear functions. Some precise numerical values of them are given in Table 5.

3.3. CHORDWISE BENDING VIBRATION ANALYSIS INCLUDING THE COUPLING EFFECT

If the gyroscopic coupling terms are not truncated from equations (18) and (19), the two coupled equations should be used simultaneously for the vibration analysis. Along with the dimensionless variables defined in the previous sections, another parameter is defined as follows.

$$\alpha \triangleq \left(\frac{AL^2}{I_{zz}}\right)^{1/2} \tag{47}$$

α, often called the slenderness ratio, is proportional to the length to thickness ratio of a beam. Now the following dimensionless equations of motion are used for the vibration analysis. The right-hand side terms in equation (18) are neglected in equation (48) for the free vibration analysis.

$$\sum_{j=1}^{\mu} \left[M_{ij}^{11} \ddot{\theta}_j - 2\gamma M_{ij}^{12} \dot{\theta}_j + (\alpha^2 K_{ij}^S - \gamma^2 M_{ij}^{11})\theta_j \right] = 0 \tag{48}$$

$$\sum_{j=1}^{\mu} \left[M_{ij}^{22} \ddot{\theta}_j + 2\gamma M_{ij}^{21} \dot{\theta}_j + \{K_{ij}^{B2} + \gamma^2 (K_{ij}^{G2} - M_{ij}^{22})\}\theta_j \right] = 0 \tag{49}$$

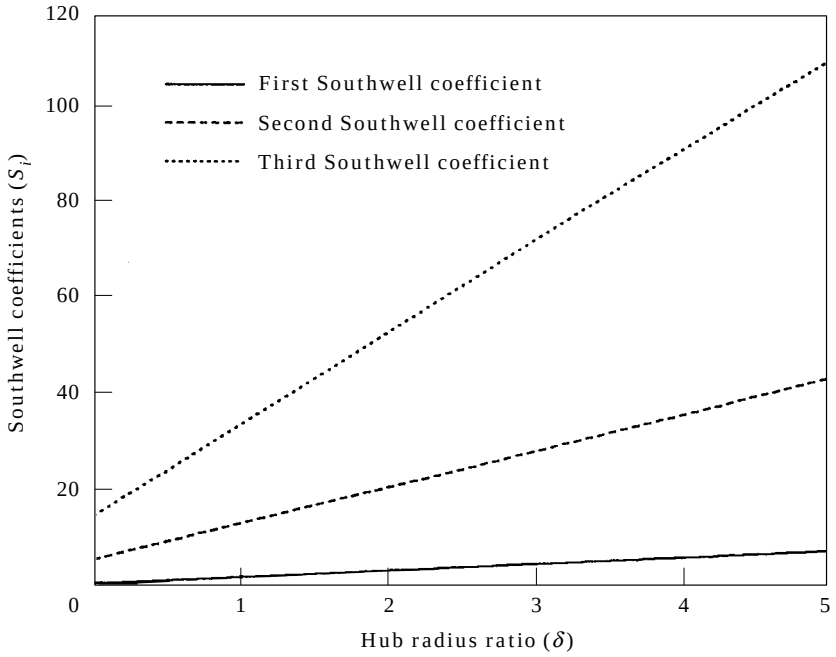

Figure 8. Southwell coefficients vs hub radius ratio.

where

$$K_{ij}^{S} \triangleq \int_0^1 \psi_{1i,\xi}\, \psi_{1j,\xi}\, \mathrm{d}\xi. \tag{50}$$

Equations (48) and (49) can be expressed as a matrix equation.

$$\mathbf{M}\ddot{\theta} + \mathbf{C}\dot{\theta} + \mathbf{K}\theta = 0 \tag{51}$$

TABLE 5

Southwell coefficients vs hub radius ratio

δ	S_1	S_2	S_3
0·0	0·0217	5·112	14·37
0·2	0·3229	6·695	18·31
0·4	0·6212	8·264	22·21
0·6	0·9180	9·826	26·09
0·8	1·214	11·38	29·96
1·0	1·509	12·94	33·83
1·2	1·804	14·49	37·69
1·4	2·098	16·04	41·55
1·6	2·393	17·59	45·41
1·8	2·687	19·14	49·27
2·0	2·981	20·69	53·12

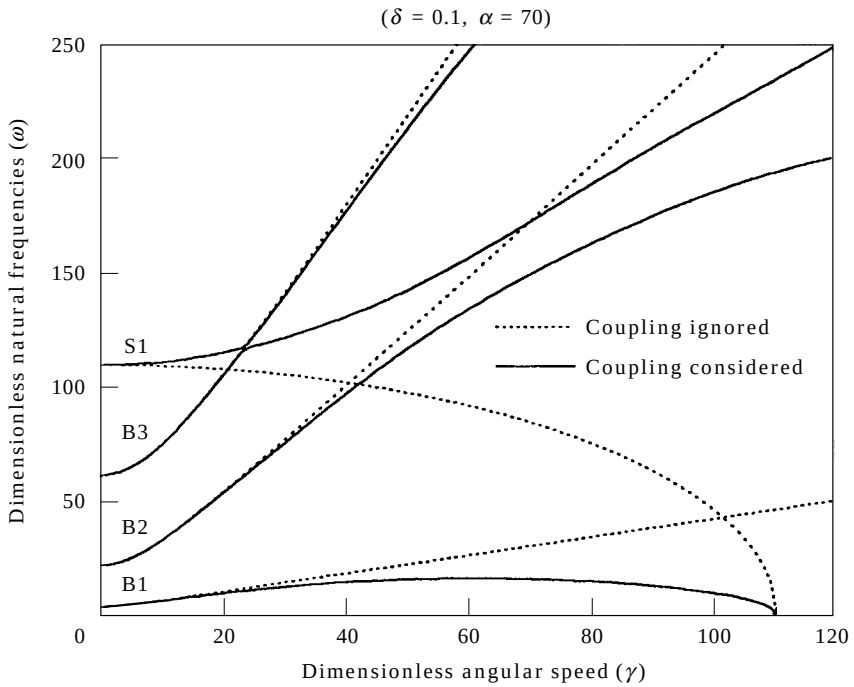

Figure 9. Coupling effect on the natural frequency variations.

where

$$\mathbf{M} \triangleq \begin{bmatrix} \mathbf{M}^{11} & 0 \\ 0 & \mathbf{M}^{22} \end{bmatrix} \tag{52}$$

$$\mathbf{C} \triangleq \begin{bmatrix} 0 & -2\gamma\mathbf{M}^{12} \\ 2\gamma\mathbf{M}^{21} & 0 \end{bmatrix} \tag{53}$$

TABLE 6

Comparison of the first chordwise natural frequencies with and without the coupling effect

δ	γ	Coupling ignored	Coupling included	Error (%)
0	2	3·62	3·62	0
	10	5·05	4·97	1·58
	50	10·5	7·55	28·1
1	2	4·40	4·40	—
	10	13·3	13·1	1·50
	50	61·6	41·4	32·8
5	2	6·65	6·64	0·15
	10	27·7	27·3	1·44
	50	136	74·2	45·4

$$\mathbf{K} \triangleq \begin{bmatrix} \alpha^2\mathbf{K}^S - \gamma^2\mathbf{M}^{11} & 0 \\ 0 & \mathbf{K}^{B2} + \gamma^2(\mathbf{K}^{G2} - \mathbf{M}^{22}) \end{bmatrix} \tag{54}$$

where $\mathbf{M}^{ab}$, $\mathbf{K}^S$, $\mathbf{K}^{B2}$ and $\mathbf{K}^{G2}$ are the matrices which have M_{ij}^{ab}, K_{ij}^S, K_{ij}^{B2}, and K_{ij}^{G2} as their elements, respectively. Since matrix $\mathbf{C}$ is not symmetric, the real modal analysis method (used in the previous section) cannot be used for equation (51). In order to use a complex modal analysis method, equation (51) is transformed into the following form.

$$\mathbf{A}\dot{\mathbf{z}} + \mathbf{B}\mathbf{z} = 0 \tag{55}$$

where

$$\mathbf{A} \triangleq \begin{bmatrix} \mathbf{M} & 0 \\ 0 & \mathbf{I} \end{bmatrix} \tag{56}$$

$$\mathbf{B} \triangleq \begin{bmatrix} \mathbf{C} & \mathbf{K} \\ -\mathbf{I} & 0 \end{bmatrix} \tag{57}$$

$$\mathbf{z} \triangleq \begin{Bmatrix} \dot{\theta} \\ \theta \end{Bmatrix} \tag{58}$$

where $\mathbf{I}$ represents a unit matrix. From equation (55), an eigenvalue problem can be derived by assuming that $\mathbf{z}$ is a harmonic matrix function of τ expressed as

$$\mathbf{z} = \mathrm{e}^{\sigma\tau}\mathbf{Z} \tag{59}$$

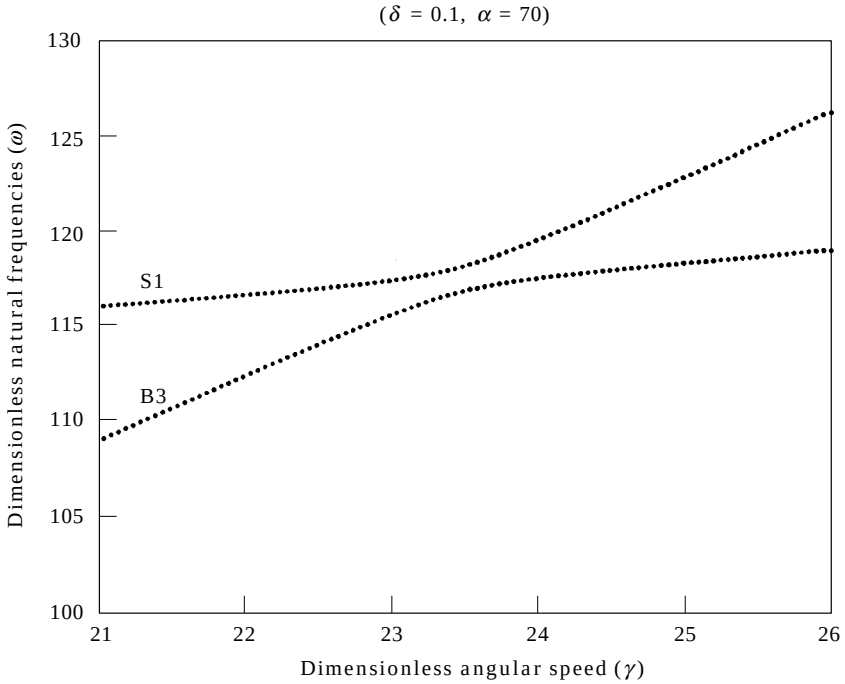

Figure 10. Magnificient of the abrupt veering region.

where σ is the complex eigenvalue and $\mathbf{Z}$ is the complex mode shape. Substitution of equation (59) into equation (55) yields

$$\sigma \mathbf{AZ} + \mathbf{BZ} = 0. \tag{60}$$

Ten stretching and ten bending modes are used to obtain the numerical results shown in Figure 9. The lowest four natural frequency loci are plotted with solid lines in the figure. Dimensionless variables of $\delta = 0{\cdot}1$ and $\alpha = 70$ are used. The value of $\alpha = 70$ guarantees the assumption of Eulerian beam (to neglect shear and rotary inertia effects). The dotted lines in the figure represent the results of ignoring the coupling terms. At $\gamma = 0$, the first three of them represent the lowest three bending natural frequencies and the fourth represents the first stretching natural frequency. In the results obtained by ignoring the coupling effect, the bending natural frequencies increase and the stretching frequency decreases as the angular speed increases. However, this is not true when the coupling effect

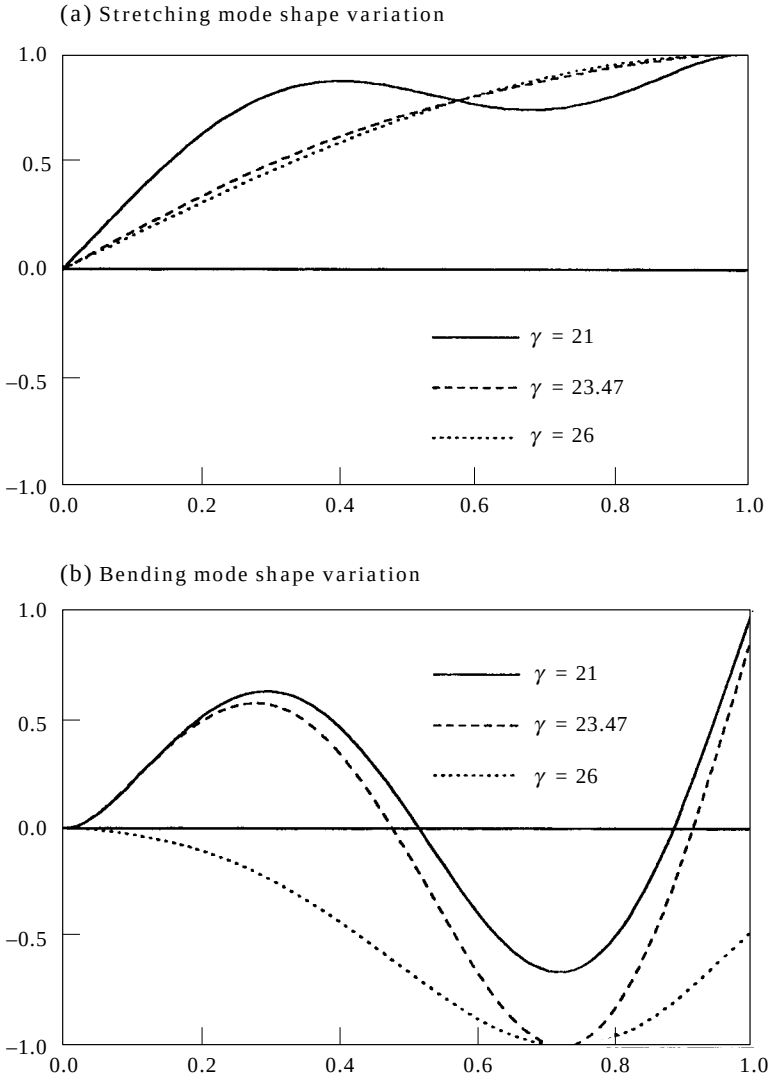

Figure 11. Mode shape variations along the third locus (in the abrupt veering region).

is included. For instance, the first bending natural frequency does not increase monotonically. The difference between the solid lines and dotted lines, however, remains insignificant when the angular speed ratio is small (roughly <10). Table 6 shows the difference quantitatively. When the coupling effect is included, there exists an angular speed where the first bending natural frequency becomes zero. Note that the first stretching natural frequency becomes zero at the same angular speed when the coupling effect is ignored. The rotating cantilever beam will buckle at the zero natural frequency. The angular speed will be called, herein, the buckling speed. The buckling speed has relation with the slenderness ratio α. The buckling speed, however, has nothing to do with the hub radius ratio. Since the buckling speed is proportional to α, the increment of slenderness ratio results in the increment of the buckling speed. This might sound weird since the beam becomes more fragile as it becomes slender. However, the centrifugal inertia force (which

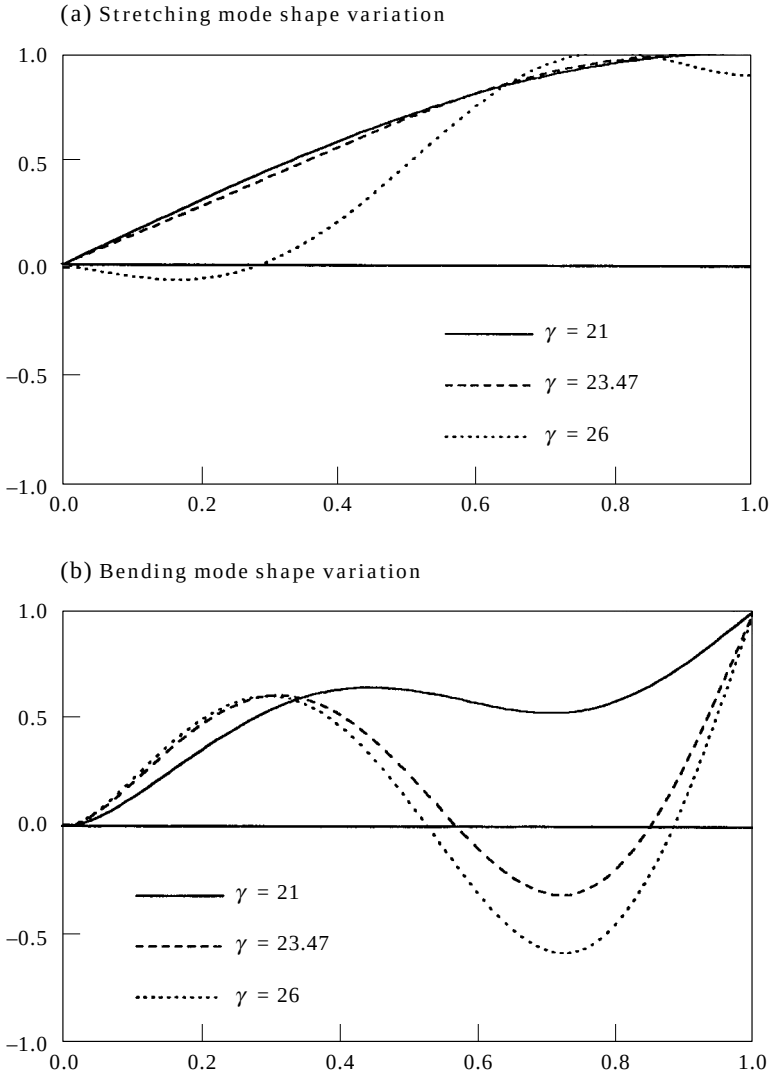

Figure 12. Mode shape variations along the fourth locus (in the abrupt veering region).

plays the role to buckle the beam) also decreases as the beam becomes slender. The discrepancy between the results obtained by ignoring the coupling effect and those by including the coupling effect decreases at an angular speed if the buckling speed increases. This implies that the coupling effect becomes less significant as the slenderness ratio of the beam increases.

Another interesting phenomenon can be observed in Figure 9. The two eigenvalue loci (third and fourth) veer at $\gamma = 23{\cdot}8$. The veering region, magnified in Figure 10, clearly shows that the two loci veer rather than cross. The variations of the two veering mode shapes are shown in Figures 11 and 12. Stretching and bending mode shapes are plotted in the figures. As the angular speed increases, the mode shapes change abruptly around the veering region. Another veering exists between the second and the third bending freuqency loci. Different from the previous one, this veering occurs gradually. The corresponding mode shape variations are shown in Figures 13 and 14.

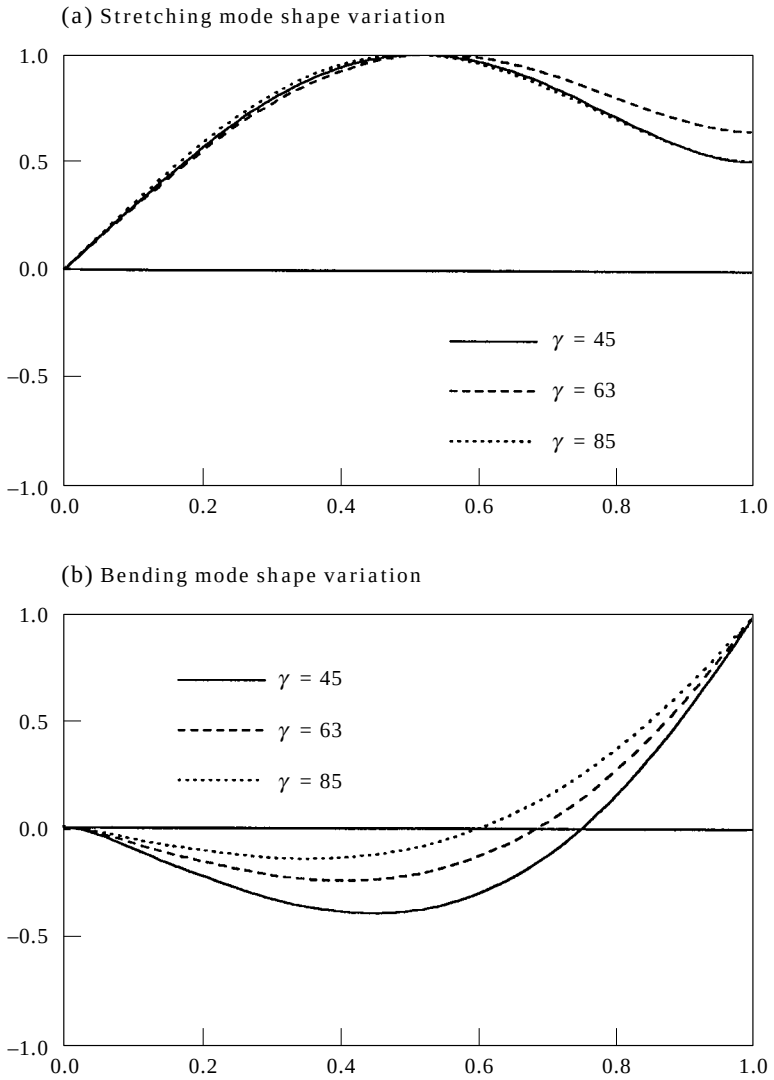

Figure 13. Mode shape variations along the second locus (in the gradual veering region).

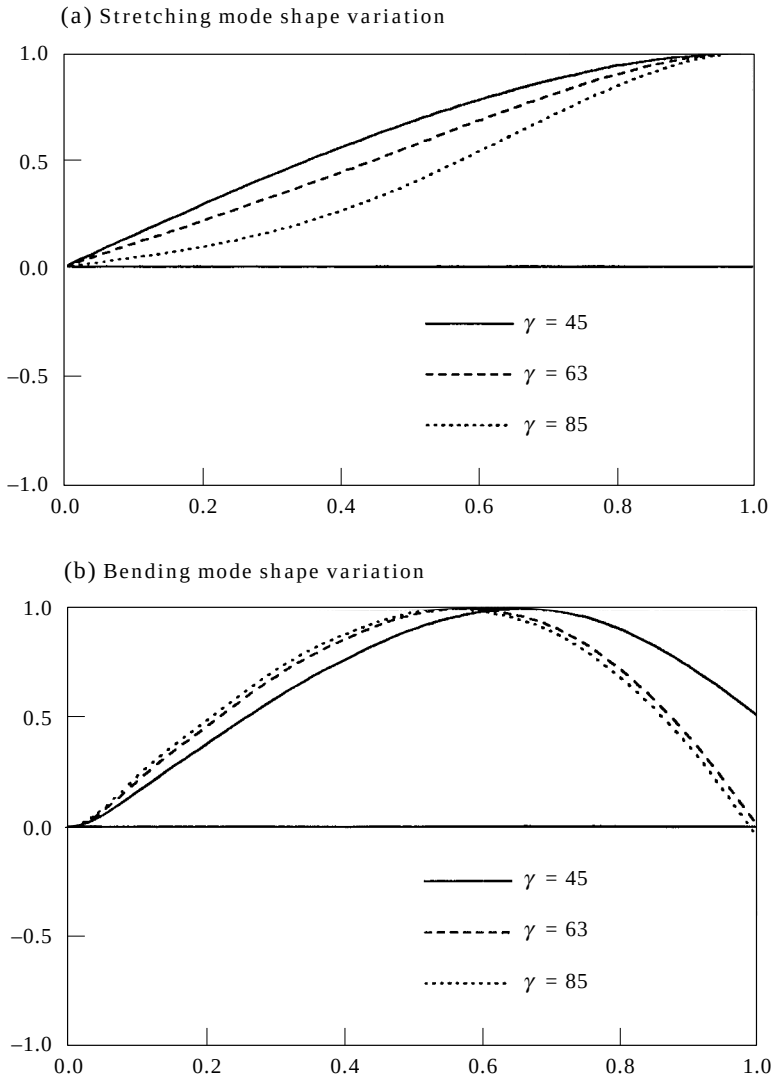

Figure 14. Mode shape variations along the third locus (in the gradual veering region).

4. CONCLUSION

In this paper, three sets of linear equations of motion for rotating cantilever beams were derived based on a new dynamic modelling method. By using the set governing flapwise bending motion which was uncoupled with other two sets, flapwise bending vibration analyses were performed. The natural frequencies were shown to increase as the angular speed and the hub radius increased. It was verified that the tuned angular speed did not exist in the flapwise bending vibration. The equation set governing chordwise bending motion was shown to be coupled with the set governing stretching motion. When the coupling effect was ignored, the behaviour of the natural frequency loci was similar to the one obtained from the flapwise bending vibration. However, the tuned angular speed was shown to exist in the chordwise bending vibration. A modal formulation to obtain the tuned angular speed was derived. When the coupling effect was considered, quite different natural frequency loci were exhibited, especially in the high angular speed region. The

buckling speed and natural frequency loci veering phenomena were observed. It was proved that the coupling effect became negligible as the slenderness ratio of the beam increased.

ACKNOWLEDGEMENT

This work is supported by Korea Ministry of Education through the Research Fund (01E0937), for which the authors are grateful.

REFERENCES

1. Southwell and Gough 1921 *British A.R.C. Report and Memoranda No*. 766. The Free transverse vibration of airscrew blades.
2. F. Liebers 1930 *NACA TM No*. 568. Contribution to the theory of propeller vibrations.
3. T. Theodorsen 1950 *NACA TN No*. 516. Propeller vibrations and the effect of centrifugal force.
4. M. Schilhansl 1958 *Journal of Applied Mechanics*, *Transactions of the American Society of Mechanical Engineers* **25**, 28–30. Bending frequency of a rotating cantilever beam.
5. S. Putter and H. Manor 1978 *Journal of Sound and Vibration* **56**, 175–185. Natural frequencies of radial rotating beams.
6. R. Bhat 1986 *Journal of Sound and Vibration* **105**, 199–210. Transverse vibrations of a rotating uniform cantilever beam with tip mass as predicted by using beam characteristic orthogonal polynomials in the Rayleigh–Ritz method.
7. D. Hodges 1979 *Journal of the American Helicopter Society* **24**, 43–50. Vibration and response of nonuniform rotating beams with discontinuities.
8. S. Hoa 1979 *Journal of Sound and Vibration* **67**, 369–381. Vibration of a rotating beam with tip mass.
9. A. Wright, C. Smith, R. Thresher and J. Wang 1982 *Journal of Applied Mechanics* **49**, 197–202. Vibration modes of centrifugally stiffened beams.
10. C. Fox and J. Burdess 1979 *Journal of Sound and Vibration* **65**, 151–158. The natural frequencies of a thin rotating cantilever with offset root.
11. T. Yokoyama 1988 *International Journal of Mechanical Sciences* **30**, 743–755. Free vibration characteristics of rotating Timoshenko beams.
12. S. Naguleswaran 1994 *Journal of Sound and Vibration* **176**, 613–624. Lateral vibration of a centrifugally tensioned Euler–Bernoulli beam.
13. S. Lee and S. Lin 1994 *Journal of Applied Mechanics* **61**, 949–955. Bending vibrations of rotating nonuniform Timoshenko beams with an elastically restrained root.
14. A. Leissa 1981 *Applied Mechanics Reviews* **34**, 629–635. Vibrational aspects of rotating turbomachinery blades.
15. C. Eick and M. Mignolet 1995 *AIAA Journal* **33**, 528–538. Vibration and buckling of flexible rotating beams.
16. H. Frisch 1975 *NASA TN D*-8047. A vector-dyadic development of the equations of motion for N-coupled flexible bodies and point masses.
17. J. Ho 1977 *Journal of Spacecraft and Rockets* **14**, 102–110. Direct path method for flexible multibody spacecraft dynamics.
18. T. Kane, R. Ryan and A. Banerjee 1987 *Journal of Guidance*, *Control*, *and Dynamics* **10**, 139–151. Dynamics of a cantilever beam attached to a moving base.
19. H. Yoo, R. Ryan and R. Scott 1995 *Journal of Sound and Vibration* **10**, 139–148. Dynamics of flexible beams undergoing overall motions.
20. L. Eisenhart 1947 *An Introduction to Differential Geometry*. Princeton University Press.